Simulation of Homogeneous and Incompressible Çinlar Flows

Mine Çağlar

Princeton University, Princeton, NJ USA[1]

We study the simulation of stationary, homogeneous, incompressible and isotropic Çınlar flows on $\mathbb{R}^2$. The flow is generated by a velocity field obtained by the superposition of vortices of rotation. The arrival time and location of vortices form a Poisson point process. The two stages of the simulation of the flow are the generation of the velocity field and the integration of the particle paths. We generate the velocity field on a bounded domain D exactly. The velocity field on D is fully described by the parameters of vortices that are stored in a stack the size of which is fairly stable at the stationary regime. We obtain the particle path by integrating the flow equation using a fourth order Runge-Kutta method. A range of ratios of the two relevant time scales lead to a variety of particle paths. Under some regimes, the paths are nearly Brownian, under other, the paths are clearly circular with some drift. Finally, we compute single particle dispersion, Lagrangian autocorrelation, and diffusivity estimators through Monte Carlo simulations. The results are useful for fitting the model to real data.

Key Words: Simulation, stochastic flows, Poisson shot-noise, dispersion.

1 Introduction

We investigate the simulation of flows generated by a class of velocity fields recently introduced by Çinlar.[1,2] Such velocity fields are vector field-valued versions of Poisson shot-noise and are close to those used in discrete vortex methods. But they have superior qualities: they are stationary and ergodic, and can be made homogeneous, incompressible and isotropic easily by

[1]Current address: Koç University, Istanbul, Turkey

means of a more general definition of a vortex. We focus on flows on $\mathbb{R}^2$ with all of these properties in the present paper, a preliminary version of which has appeared elsewhere.[3]

Let v be a deterministic velocity field called the *basic vortex*, and let $Q = \mathbb{R}^2 \times \mathbb{R} \times (0, \infty)$ be an index set. We obtain *vortices* for $q \in Q$ by

$$v_q(x) = a\, v(\frac{x - z}{b}) \qquad \text{for} \quad q = (z, a, b)\ . \tag{1}$$

Let N be a Poisson random measure on the Borel sets of $\mathbb{R} \times Q$ with mean measure

$$\mu(dt, dz, da, db) = \lambda\, dt\, dz\, \alpha(da)\beta(db) \tag{2}$$

where λ is the arrival rate per unit time-unit space, and α and β are probability distributions. The arrival time t of a vortex, its location z in space, its amplitude a as well as its dilation factor b are all random and governed by N. By the superposition of these vortices appropriately decaying in time, a stationary velocity field u is constructed[1] as

$$u(x, t) = \int_{(-\infty, t] \times Q} N(ds, dz, da, db)\, \mathrm{e}^{-c(t-s)}\, a\, v(\frac{x - z}{b}) \qquad x \in \mathbb{R}^2, \quad t \in \mathbb{R} \tag{3}$$

where $c > 0$ is the decay parameter.

The path $\{X_t : t \geq 0\}$ of a particle that started at x at time 0 is the solution of the ordinary differential equation

$$\frac{d}{dt} X_t = u(X_t, t) \qquad X_0 = x\ . \tag{4}$$

Our aim is to simulate a variety of particle paths and hence explore the parameters of the velocity model (3). In Section 2, the details of the velocity model is outlined. In Section 3, we investigate the typical length and time scales. The identification of these scales serves as a general guide for comparing different models and putting numerical values into physical perspective. The typical paths are simulated in Section 4 for a range of ratios of the time scales while keeping the length scale constant. Each ratio appears to represent a different regime of motion.

In the last two decades, Lagrangian data have been extensively used to describe the characteristics of flows in several regions of ocean.[4] The positions of current following surface drifters, fixed by the sensors on satellites, provide the data. In stationary and homogeneous regions, the observations are used to obtain single particle dispersion, Lagrangian autocorrelation, and

diffusivity estimators.[5] We explore these basic indicators in Çinlar flows through Monte Carlo simulations in Section 5, as an extension of the results of Section 4. Finally, we deduce a framework for matching the parameters of the flow model to real data.

2 Homogeneous and Isotropic Velocity Field

In this section, we review some details of the velocity field

$$u(x,t) = \int_{(-\infty,t]\times Q} N(ds,dz,da,db)\, \mathrm{e}^{-c(t-s)}\, a\, v(\frac{x-z}{b}) \qquad x \in \mathbb{R}^2,\ \ t \in \mathbb{R} \tag{5}$$

as given in references 1 and 2. It is stationary, homogeneous and isotropic according to the following definitions. A velocity field u is said to be *stationary* (in the strict sense) if, for each $x \in \mathbb{R}^d$, the distribution of the collection $\{u(x, s+t) \,:\, t \in \mathbb{R}\}$ is the same for all $s \in \mathbb{R}$. A velocity field u is called *homogeneous* in space if, for each $t \in \mathbb{R}$, the probability law of the collection $\{u(z+x,t) \,:\, x \in \mathbb{R}^d\}$ is the same for all $z \in \mathbb{R}^d$. That is, the probability law of u_t is invariant under translations of the space $\mathbb{R}^d$. Isotropy corresponds to invariance of the same law under rotations and reflections of the coordinate system. Precisely, u is called *isotropic* if it is homogeneous and for each t the probability laws of $\{u(Gx,t) \,:\, x \in \mathbb{R}^d\}$ and $\{G\,u(x,t) \,:\, x \in \mathbb{R}^d\}$ are the same for all orthogonal transformations G of $\mathbb{R}^d$.

The verification of these properties rely on the characteristic function formula

$$\mathbb{E}\, \exp i \int N(dr) f(r) = \exp \int \mu(dr)(e^{if(r)} - 1) \tag{6}$$

about integrals with respect to Poisson random measures[6] since the velocity field (5) is such an integral. The finite dimensional distributions of u, that is, the distributions of

$$u(x_1,t), u(x_2,t), \ldots, u(x_n,t) \qquad x_1, \ldots, x_n \in \mathbb{R}^d$$

determine the distribution of the collection $\{u(x,t) \,:\, x \in \mathbb{R}^d\}$. The characteristic function for such distributions is computed[1,2] through the use of formula (6) and is given by

$$\begin{aligned} &\mathbb{E}\, \exp i \int_{\mathbb{R}^d} \gamma(dx) \cdot u(x,t) \\ &\quad = \exp\, - \textstyle\int_{\mathbb{R}_+\times Q} \mu(dt,dq)[1 - \exp ie^{-cs} \int_{\mathbb{R}^d} \gamma(dx) \cdot v_q(x)] \end{aligned}$$

where dot denotes inner product and the measure γ has the form

$$\int_{\mathbb{R}^d} \gamma(dx) \cdot f(x) = \sum_{i=1}^{n} r_i \cdot f(x_i)$$

for vectors $r_1, \ldots, r_n \in \mathbb{R}^d$. Then, the mean measure (2) and the form (1) of the vortices are taken into account to verify the above properties.

Since (5) is homogeneous[2] in space the covariance function R depends only on time and space lag, and is given by

$$\begin{aligned} R^{ij}(x,t) &= \mathbb{E}\, u^i(y,s) u^j(y+x, t+s) \\ &= \frac{1}{2c}\, e^{-c|t|}\, \lambda \int_{\mathbb{R}} \alpha(da)\, a^2 \int_{\mathbb{R}_+} \beta(db)\, b^2 \int_{\mathbb{R}^2} dz\, v^i(z)\, v^j(z + \frac{x}{b}) \end{aligned} \tag{7}$$

where $x, y \in \mathbb{R}^2$, $s, t \in \mathbb{R}$, $i, j = 1, 2$. This is computed by the use of the following formulas for the expectations and variances of integrals with respect to Poisson random measures[6]

$$\mathbb{E} \int N(dr)\, f(r) = \int \mu(dr)\, f(r)$$

and

$$\mathbb{E} \int \tilde{N}(dr) \int \tilde{N}(dr')\, f(r)\, g(r') = \int \mu(dr)\, f(r)\, g(r)$$

where $\tilde{N}(dr) = N(dr) - \mu(dr)$.

Since the flows considered in this paper are in $\mathbb{R}^2$, isotropy requires the basic vortex v to have a specific form. Namely, $v = (v^1, v^2)$ corresponds to rotation around 0 with magnitude $m(r)$ at distance r from 0. The specific equations for v are

$$\begin{aligned} v^1(x) &= \frac{x^2}{r}\, m(r) \\ v^2(x) &= \frac{x^1}{r}\, m(r) \end{aligned} \tag{8}$$

where $x = (x^1, x^2)$ and $r = |x| \in [0, 1]$. As a rotation on $\mathbb{R}^2$, v is incompressible, that is, divergence free. We let it vanish outside the unit disk. Then, every vortex is a rotation, since it is translation, amplification and dilation of v. As a superposition of these *eddies*, the velocity field u is both incompressible and isotropic.

3 Length and Time Scales

In this section, we follow the length and time scale definitions of Piterbarg,[7] given in terms of the spectral density of a stationary, homogeneous and isotropic velocity field. We compute these in terms of the covariance tensor R, which is explicit in the velocity model of Section 2. Following the usual convention, we take $(R^{11}(0,0) + R^{22}(0,0))^{1/2}$ to be the typical velocity. In absence of isotropy, the definitions can be modified to account for each spatial direction.

3.1 Length Scale

In a stationary, homogeneous and isotropic velocity field, the spectral density tensor[8] can be written in terms of two spectral densities E_L and E_N as

$$E^{ij}(k,w) = E_L(|k|,w)(\delta_{ij} - \frac{k_i k_j}{|k|^2}) + E_N(|k|,w)\frac{k_i k_j}{|k|^2} \tag{9}$$

where $|k| = k_1^2 + k_2^2$. The covariance tensor R is given by

$$R^{ij}(x,t) = \int_{\mathbb{R}} \int_{\mathbb{R}^2} \mathrm{e}^{i(k\cdot x + wt)} E^{ij}(k,w)\, dk\, dw \tag{10}$$

Piterbarg[7] assumes that $E_N = 0$ and defines a length scale l by

$$l = \left(\frac{\int\int |k| E_L(|k|,w)\, d|k|\, dw}{\int\int |k|^3 E_L(|k|,w)\, d|k|\, dw} \right)^{1/2} \tag{11}$$

We write this definition in terms of the covariance matrix R, and thus E_N is not necessarily 0 in our definitions. From (9), $E^{ii}(k,w) = E_L(|k|,w)\ (1 - k_i^2/|k|^2)$ (with $E_N = 0$), and hence from (10)

$$f(x) \equiv R^{11}(x,0) + R^{22}(x,0) = \int_{\mathbb{R}} \int_{\mathbb{R}^2} \mathrm{e}^{ik\cdot x} E_L(|k|,w)\, dk\, dw \quad . \tag{12}$$

Changing $k = (k_1, k_2)$ to polar coordinates and evaluating at $x = 0$, we get

$$R^{11}(0,0) + R^{22}(0,0) = 2\pi \int_{\mathbb{R}} \int_{\mathbb{R}_+} |k| E_L(|k|,w)\, d|k|\, dw \quad . \tag{13}$$

Then, we compute from (12) that

$$\begin{aligned} \partial_1^2 f(0) + \partial_2^2 f(0) &= -\int_{\mathbb{R}} \int_{\mathbb{R}^2} (k_1^2 + k_2^2) E_L(|k|,w)\, dk\, dw \\ &= -2\pi \int_{\mathbb{R}} \int_{\mathbb{R}_+} |k|^3 E_L(|k|,w)\, d|k|\, dw \quad . \end{aligned} \tag{14}$$

where $\partial_i^2 \equiv \partial^2/\partial x_i^2$. From (11), (13) and (14), it follows that the length scale l is given by

$$l = \left(\frac{R^{11}(0,0) + R^{22}(0,0)}{-[\partial_1^2(R^{11}(x,0) + R^{22}(x,0)) + \partial_2^2(R^{11}(x,0) + R^{22}(x,0))]_{x=0}} \right)^{1/2}$$

in terms of the covariance tensor R. Here, units of 'velocity squared' is divided by units of '1/(time squared)', and then the square root is taken, so l is in units of length. Another way of defining a length scale could be by taking the derivative of f only once to have a quantity in units of 'accelaration', and then divide f which is in units of 'velocity squared' by this, to get a quantity in units of 'length'. See for example Ref. 9, pg.51. However, the previous approach takes advantage of isotropy and the quantities are simpler to evaluate. Indeed, from (7) and (8) we get

$$\begin{aligned} R^{11}(0,0) + R^{22}(0,0) &= \frac{\lambda}{2c} \int_{\mathbb{R}} \alpha(da) \int_{\mathbb{R}_+} \beta(db)\, a^2 b^2 \int_B dz\, m^2(r) \frac{(z^1)^2 + (z^2)^2}{r^2} \\ &= \frac{\lambda\pi}{c} \int \alpha(da)\, a^2 \int \beta(db)\, b^2 \int_0^1 dr\, r\, m^2(r) \end{aligned}$$

where $r = |z|$ and B is the closed unit ball in $\mathbb{R}^2$. We also compute the quantity in (14) to get

$$\partial_1^2 f(0) + \partial_2^2 f(0) = \frac{\lambda\pi}{c} \int \alpha(da)\, a^2 \int_0^1 dr\, r\, m(r)(m''(r) + m'(r)/r - m(r)/r^2)\ .$$

Hence,

$$l = \left(\frac{\int \beta(db) b^2 \int_0^1 dr\, r\, m^2(r)}{-\int_0^1 dr\, r\, m(r)(m''(r) + m'(r)/r - m(r)/r^2)} \right)^{1/2} .$$

3.2 Time Scales

The typical time scale τ_T is defined[7] as the ratio of the length scale l to the typical velocity

$$\tau_T = \frac{l}{(R^{11}(0,0) + R^{22}(0,0))^{1/2}}$$

called the *turnover time*. From the computations of the previous subsection, we get

$$\tau_T = \left[-\frac{\lambda\pi}{c} \int \alpha(da) a^2 \int_0^1 dr\, r\, m(r)(m''(r) + m'(r)/r - m(r)/r^2) \right]^{-1/2} .$$

Another time scale is defined[7] by

$$\tau_E = \frac{\int |k| E_L(|k|, 0)\, d|k|}{\int\int |k| E_L(|k|, w)\, d|k|\, dw}$$

called *Eulerian correlation time*, or lifetime of an eddy. Working in terms of R again, we have

$$\int_{\mathbb{R}^2} \mathrm{e}^{ik\cdot x} E^{ii}(k,w)\,dk = \frac{1}{2\pi}\int_{\mathbb{R}} \mathrm{e}^{-iwt} R^{ii}(x,t)\,dt$$

by inverting the Fourier transform (10). Putting $x = 0,\ w = 0$, recalling that $E^{11}(k,0) + E^{22}(k,0) = E_L(|k|,0)$, and changing to polar coordinates, we get

$$2\pi\int_{\mathbb{R}_+} |k| E_L(|k|,0)\,d|k| = \frac{1}{2\pi}\int_{\mathbb{R}} [R^{11}(0,t) + R^{22}(0,t)]\,dt \quad .$$

Then, from (13) we can write

$$\tau_E = \frac{1}{2\pi}\int_{\mathbb{R}} [R^{11}(0,t) + R^{22}(0,t)]\,dt \;/\; [R^{11}(0,0) + R^{22}(0,0)] \quad .$$

From (7), we find

$$\tau_E = \frac{1}{2\pi}\int_{\mathbb{R}} \mathrm{e}^{-c|t|} dt = \frac{1}{\pi c} \quad .$$

The Eulerian correlation decays exponentially, however $\tau_E = 1/\pi c$ is too small to characterize the decay time for some choices of c. Since π is just a constant, we take

$$\tau_E = \frac{1}{c}$$

in our computations, which are based on time scales only comparatively.

4 Simulation of Particle Paths

In this section, we simulate a variety of particle paths by separation of the time scales τ_E, τ_T and the unit time as described below. Under some regimes, the paths are nearly Brownian, under other, the paths are clearly circular with some drift.

4.1 Simulation Procedure

There are two stages in simulation: the generation of the Eulerian velocity field and numerical integration of the flow equation (4). To generate the velocity field, we rewrite (3) in the form

$$u(x,t) = \sum_{t_i \le t} e^{-c(t-t_i)} a_i\, v(\frac{x - z_i}{b_i})$$

where (t_i, z_i, a_i, b_i) are atoms of N. To get the velocity field over a bounded domain D, we first pick the desired distribution α of the a_i to have a bounded support. Let $\hat{a} > 0$ denote the maximum value that a_i can take in absolute value. Pick the desired distribution β of the b_i to have support on $(0, \hat{b}]$, where $\hat{b} > 0$. Then, to get the velocity field on D exactly, we in fact need to simulate all the vortices with centers in $E = D + \hat{b} = \{y \in \mathbb{R}^2 : |y - x| \leq \hat{b} \text{ for some } x \in D\}$. For instance, if D is the disk of radius r, then E is the disk of radius $r + \hat{b}$, both centered at 0. Let $\hat{\lambda}$ be the intensity λ multiplied by the area of E. We generate the times $t_1, t_2, \ldots$ to be the arrival times of a Poisson process with rate $\hat{\lambda}$. To each t_i, we associate the random point z_i with the uniform distribution over E. Then, we take a_i from the distribution α and b_i from the distribution β. This specifies $u(x,t)$ for all $x \in D$ and $t \geq 0$. We store the t_i, z_i, a_i and b_i for each vortex, but only until the vortex decays to negligible magnitude, that is, until the first time $t > t_i$ such that $\mathrm{e}^{-c(t-t_i)}|a_i|$ is very small, so small that this quantity times λ is still small, otherwise the sum $u(x,t)$ can be large for large values of λ. We conclude that the velocity field reaches the stationary regime at the first time $t^* > 0$ that makes $\lambda\,\mathrm{e}^{-ct^*}|\hat{a}|$ negligible. Indeed, the number of vortices that are kept in our stack is fairly stable after t^*. In the generation of the velocity field, there is no discretization of time or space, so numerical errors come only from machine precision and the killing of vortices, which are both negligible.

We place a particle in D at time t^* and relabel the time as 0. The observation time $\hat{t}$ is predetermined according to typical length and time scales so that it is probably less than the first hitting time of the particle to the boundary of D. Then, the computation of the particle path is a deterministic integration over the realization of the velocity field in time $[0, \hat{t}]$. We use the fourth order Runge-Kutta method[10] to solve (4). Precisely, let h be the integration time step. We compute in turn

$$\begin{aligned}
k_1 &= h\,u(x_n, t_n) \\
k_2 &= h\,u(x_n + \frac{k_1}{2}, t_n + \frac{h}{2}) \\
k_3 &= h\,u(x_n + \frac{k_2}{2}, t_n + \frac{h}{2}) \\
k_4 &= h\,u(x_n + k_3, t_n + h) \\
x_{n+1} &= x_n + \frac{1}{6}(k_1 + 2k_2 + 2k_3 + k_4)
\end{aligned}$$

with $x_0 = x$. Since the velocity field jumps at arrival times of the Poisson process (remaining continuous in x), the discretization of time is done accordingly. Each time we move the particle, we need to compute the Lagrangian velocity $u(X_t, t)$ by searching our data structure for the vortices. It is sufficient to search for vortices with centers within a radius $\hat{b}$ of the particle. The velocity field $u(x,t)$ is continuous in x, and it is infinitely differentiable in t between jumps. Therefore, the discretization error is of $\mathrm{O}(h^5)$ as usual for the fourth order Runge-Kutta method. In the next section, the numerical values of h and $\hat{t}$ are chosen so that the particle paths are invariant over $[0, \hat{t}]$ for those and smaller values of h.

We fix the length scale by fixing the distribution β of the b_i and the magnitude function m. We select α from a one-parameter family of distributions. Then, the inputs to the simulation program are only c, λ, $\hat{t}$ and the parameter of α. The program is coded in the C programming language, and it is executed on Silicon Graphics machines. For most parameter choices, the program runs very fast. The output is the particle position at every time step.

4.2 Particle Paths

We select β to be a discrete distribution with the following probability mass function

$$p(0.5) = 8/15, \qquad p(1) = 4/15, \qquad p(1.5) = 2/15, \qquad p(2) = 1/15\ . \tag{15}$$

This fixes the length scale l to be 0.235. We visualize the flow on a disk of radius $50\,l \approx 11$, which is reasonably large. We take α to be the uniform distribution on $[-\hat{a}, \hat{a}]$. We select the magnitude function m by

$$m(r) = \frac{1 - \cos 2\pi r}{2} \qquad 0 \le r \le 1$$

and $m(r) = 0$ otherwise.

Every choice of the input parameters yields different time scales τ_E and τ_T. Since the length scale is fixed, we concentrate only on the ratio of the time scales τ_E/τ_T. This is roughly the 'number of turns' in one Eulerian time by which the velocity field decays considerably. We study the ratios 0.1, 1, 10 and 100, and separate the scales τ_T, τ_E and 1 (unit time) within the same ratio. In all cases, the time step h is chosen so small that the particle paths converge. Precisely,

we have

$$\max_n |x_n(h) - x_n(h')| \leq 0.1 \qquad \text{for } h' \leq h \tag{16}$$

Typically, h varies from 0.1 to 0.001 in the particle paths generated over $[0, \hat{t}]$ below.

The results are given in Figures 1 through 9 where the relation $x \ll y$ means y is 10 times x in magnitude for real valued quantities x and y. The figures span all possible separation of scales except for one family. We have not displayed the cases where $\tau_T \gg 1$ (except for Figure 1). When $\tau_T \gg 1$, the particle has to be moved very slowly, for a very long time. This is basically because τ_T is the typical time; to observe motion we have to wait for several units of τ_T. We omit this case as the ratio $\tau_E \,/\, \tau_T$ is more important and is explored in other cases.

Figures 1,2,3 correspond to ratio $\tau_E \,/\, \tau_T = 0.1$, Figures 4, 5 to $\tau_E \,/\, \tau_T = 1$, Figures 6, 7, 8 to $\tau_E \,/\, \tau_T = 10$, and Figure 9 to $\tau_E \,/\, \tau_T = 100$. We observe that the number of turns increases as the ratio increases as expected. The rotations are very obvious for $\tau_E \,/\, \tau_T = 10, 100$. Yet, every picture within the same ratio looks qualitatively different as the time unit varies. For instance, as c increases the paths start to look more irregular and less smooth for each fixed ratio. This suggests that the particle behaves more like a Brownian particle when the decay rate c increases, which is observed especially for ratios 0.1 and 1. In the case of $\tau_E \,/\, \tau_T = 10$, the particle is locked to an eddy for some time for the smallest value of c in Figure 6. A similar pattern is observed also for ratio 100. Finally, τ_T is indeed the typical time; the bigger it is with respect to unit time, the shorter the length of the path is within the fixed domain D for a fixed period.

5 Dispersion

The term *dispersion* usually refers to that of a cloud of admixture placed in fluid. The concentration of mass at all positions $x \in \mathbb{R}^d$ and times $t \in \mathbb{R}_+$ provides the complete picture and is usually studied for quantifying dispersion of an admixture. In the beginning, suppose this mass occupies a disk of finite radius, say r, around the origin. In a flow of homeomorphisms the mass is contained in this boundary at all times, but the boundary moves in time. In an incompressible flow, the area and the concentration of the mass inside the boundary remain the

same in time. However parts of the mass disperse far from distance r as prolongated extensions. This is illustrated in Figure 10, in which the parameters are the same as in Figure 4. We follow only the particles on the boundary as the flow is a homeomorphism basically by the smoothness of the basic vortex chosen.[11] We place 1000 particles on a circle of radius 3 at $t = 0$ on the stationary velocity field. When two particles get more distant than they were at the beginning, we insert another particle between them.[12] As the particles are very close to each other, this approximation is appropriate for visualization purposes. At time 35, we have 48689 particles on the boundary. Here, the time step h is 0.1 and as it is reduced the traces remain invariant. For example, the distance between corresponding particles is less than 0.05 for traces with $h = 0.1$ and $h = 0.01$, and the plots are visually indistinguishable.

We see that the probability density that a particle is found at x at time t is sometimes identified with the expected concentration of an admixture at that position and time. The heuristic argument for this is based on the assumption that all particles diffuse independently.[13] Then, when a large ensemble of particles of unit mass is released at the origin at time 0, the amount of mass at x at time t should give the desired probability. This is only approximate for large scale flows where the particles close to each other at start move closely at least for a while. Yet, single particle dispersion, which will shortly be defined as the second moment of the distribution of the particle position, is considered as an important indicator for mass dispersion.

Let X_t denote the position at time t of a particle that started at position 0 at $t = 0$. We define *single particle dispersion* as

$$\mathbb{E}\,|X_t|^2 = \mathbb{E}\,(X_t^1)^2 + \mathbb{E}\,(X_t^2)^2 \quad . \tag{17}$$

From (4), we have

$$\frac{d}{dt}\,(X_t^i)^2 = 2X_t^i\,u^i(X_t,t) = 2\int_0^t u^i(X_t,t)u^i(X_s,s)\,ds \quad . \tag{18}$$

Since u is stationary, homogeneous and incompressible, the Lagrangian velocity process $\{u(X_t,t) : t \geq 0\}$ is also stationary by Proposition 5.3.4 of Ref. 14. Let ρ denote the autocorrelation tensor of this process, called the Lagrangian autocorrelation. That is,

$$\rho^{ij}(s) = \frac{\mathbb{E}\,u^i(X_t,t)u^j(X_{t+s},t+s)}{\mathbb{E}\,u^i(0,0)u^j(0,0)} \quad .$$

Then, after integrating (18), taking expectations, and making a change of variable, we get

$$\mathbb{E}\,(X_t^i)^2 = 2\,\mathbb{E}\,u^i(0,0)^2 \int_0^t \int_0^r \rho^{ii}(s)\,ds\,dr = 2\,\mathbb{E}\,u^i(0,0)^2 \int_0^t (t-s)\rho^{ii}(s)\,ds \quad . \tag{19}$$

This is known as *Taylor's Theorem* for homogeneous and stationary turbulence in presence of which it is conjectured that the Lagrangian velocity is also a stationary process.[13] This is indeed satisfied by the velocity model (5) as described above.

Studying Equation (19), we see that as t tends to 0, $\rho(t)$ goes to 1 and

$$\mathbb{E}\,(X_t^i)^2 \;\sim\; \mathbb{E}\,u^i(0,0)^2\,t^2 \qquad \text{as } t \;\to 0 \quad .$$

On the other hand, when t is very large, we have

$$\mathbb{E}\,(X_t^i)^2 \;\sim\; 2\,\mathbb{E}\,u^i(0,0)^2\;t \int_0^\infty \rho^{ii}(s)\,ds \qquad \text{as } t \;\to \infty \tag{20}$$

if the integrals $\int_0^\infty \rho(s)\,ds$, and $\int_0^\infty s\rho(s)\,ds$ are finite. As $t \to \infty$, the particle shows diffusive behavior as in Brownian motion where second moment of the particle position grows like t.

The turbulent diffusion is usually studied through the advection diffusion equation, which is a differential equation for the expected concentration of mass. Suppose this concentration is identified with the probability density function of X_t, as described above. In this case, if the distribution of X_t is assumed to be Gaussian, the i^{th} component of the diffusion constant in the advection diffusion equation can be found to be

$$K^i = \frac{1}{2}\,\frac{d}{dt}\mathbb{E}\,(X_t^i)^2$$

where molecular diffusion is neglected. See Ref. 13, pg.62, for a derivation. From (19), we have

$$K^i = \sigma^2 \int_0^t \rho^{ii}(s)\,ds$$

where $\sigma^2 \equiv \mathbb{E}\,u^1(0,0)^2$, which is equal to $\mathbb{E}\,u^2(0,0)$ because of isotropy. In general, the quantity K^i is taken as a definition for *diffusivity* in the analysis of data from a homogeneous and stationary flow. Note that for large t, K^i is approximately equal to 1/2 times the coefficient of t in Equation (20). From (17), we have

$$\mathbb{E}\,|X_t|^2 \;\sim\; 4\,K\,t \qquad \text{as } t \to \infty \tag{21}$$

where we put $K = K^1 = K^2$ in view of isotropy.

5.1 Monte Carlo Simulation

We perform a large number, say n, of independent simulation runs in order to estimate $\mathbb{E}|X_t|^2$ of (17) by calculating

$$\overline{|X_t|^2} = \frac{1}{n}\sum_{k=1}^{n} |X_t|_k^2 \ , \tag{22}$$

where $|X_t|_k^2$ is the statistic from k^{th} run, and $X_0 = 0$. Each run is the simulation of the particle path, which is described in the previous section.

Since n is large, we have chosen "ran1.c",[15] a random number generator with a long period. In order to determine n, first we check the sample mean of $u(0,0)$, for n=1000, 2000, and 3000 runs. As the real mean $\mathbb{E}\,u(0,0)$ is 0, this analysis provides an empirical estimate of n. On the other hand, we control the accumulation of errors throughout time by checking the sample mean $\overline{X_t}$ for the period of time $\hat{t}$ that the particle is followed. The exact value is $\mathbb{E}\,X_t = 0$, for all $t \geq 0$, because

$$\mathbb{E}\,X_t = \int_0^t \mathbb{E}\,u(X_s, s)\,ds \ ,$$

which is equal to 0 because $\mathbb{E}\,u(X_s,s) = \mathbb{E}\,u(0,0) = 0$ for each s as $\{u(X_t,t) : t \in \mathbb{R}\}$ is stationary. We also compare the sum $(\overline{X_t^1})^2 + (\overline{X_t^2})^2$ with $\overline{|X_t|^2}$, for $0 \leq t \leq T$. The number n is chosen sufficiently large to make their difference at most 0.1% of $\overline{|X_t|^2}$. Note that second moment of X_t is also its variance, as its mean is 0. So, by control of this error and large choice of n, there is no significant difference between the statistics we get from the estimator in (22) and the sample variance $s^2 \equiv \sum_{k=1}^{N}(X_k - \overline{X})^2/(N-1)$.

5.2 Single Particle Dispersion

Our aim is to explore both the small time (quadratic) and the large time (linear) behavior of $\overline{|X_t|^2}$, and compute the diffusivity K. We focus on dispersion caused by turbulent eddies which have larger scales than molecular motions. In view of the results of the previous section, we select the decay rate c sufficiently small so that Eulerian velocity decorrelates slowly in time. Although we cannot compute analytically, Lagrangian autocorrelation ρ must be affected by c in a similar way. So, we select τ_E relatively high. On the other hand, we will see that a certain pattern exists for a range of values of τ_T below.

We study $\tau_T = 1$ in detail. Fixing τ_T leaves two parameters free among c, λ and $\hat{a}$. We investigate a range of these parameters as follows. We start with the parameters of Figures 4 and 6 of the previous section that correspond to $\tau_T = 1$. The estimators $\hat{\rho}^{11}$ and $\overline{|X_t|^2}$ are given in Figure 11 for the parameter set of Figure 4 where $c = 1$. We do not display $\hat{\rho}^{22}$ since it is almost identical to $\hat{\rho}^{11}$ by isotropy. Note that $\overline{|X_t|^2}$ grows linearly in time almost right from time 1. The parameter combination of Figure 6 where $c = 0.1$ has shown a similar behavior. In both of these cases, we have $\lambda/c = 0.1$ and the diffusivity K as defined in (21) is estimated to be 0.02.

Next, we reduce c to 0.01, with $\lambda = 0.01$. The autocorrelation estimator $\hat{\rho}^{11}$, and dispersion estimator $\overline{|X_t|^2}$ are given in Figure 12. Here we have faster dispersion in shorter time. The statistic $\overline{|X_t|^2}$ is clearly quadratic for small t and becomes linear after around $t = 5$ when $\hat{\rho}^{ii}$, $i = 1, 2$, become practically 0. We have also tried $c = 0.001$ with $\lambda = 0.001$. This gives almost the same result as in Figure 12. In both of these cases, we have $\lambda/c = 1$ which is 10 times that in Figure 11. Intuitively, the eddies arrive faster than they decay, and hence we are able to observe the small time behavior. For the large time behavior, the diffusivity K is 0.04, greater than that of Figure 11.

Continuing in this manner, we increase λ/c to 10. The results with $c = 0.01$ are given in Figure 13. The parameter combination $c = 0.001$ and $\lambda = 0.01$ has produced a similar output. In these cases, we have faster dispersion and higher diffusivity K 0.07. However, increasing the ratio λ/c to 100 with $c = 0.001$ and $c = 0.0001$ does not change the outlook of dispersion and the diffusivity any more, K is still 0.07. Estimators of the diffusivity K are tabulated in Table 1 for all of our experiments with $\tau_T = 1$.

The graph of dispersion together with K can be used to fit parameters to real data. To match the magnitude of K to that estimated from data, one needs to rescale the space, which has been the free dimension in our analysis. Indeed in all above experiments, the diffusivity K is around the same order of magnitude, but the graph of dispersion varies. The choice of the unit of space and rescaling it by varying the distribution β of b would adjust the value of K to the one estimated from data. An increase in length scale l when τ_T is held constant would result in higher values of diffusivity.

By the same token, to produce a wide range of orders of magnitude for K one could change the time scale τ_T while keeping the length scale constant. We expect that K will increase as τ_T decreases. With this insight, we have also conducted the following experiments with $\tau_T = 0.01, 0.1$, and 10; the graphs of dispersion are given in Figures 14, 15 and 16, respectively. The first two correspond to the parameter sets of Figures 8 and 9, respectively, and the last one is similar to those in Figure 1, all with $\lambda/c = 1$. The similarity of Figures 14 and 15 to the dispersion plot in Figure 12 is striking. In these, only the time axis is different consistent with the time scales $\tau_T = 0.01, 0.1, 1$, and all have $\lambda/c = 1$. The same similarity exists also for the corresponding autocorrelation functions.

We have plotted K versus τ_T in log-log scale in Figure 17 for all experiments performed. The order of magnitude of K increases as τ_T decreases as we expected. So, alternatively, one can change the time scale while keeping the length scale constant to fit parameters to real data. Further adjustment should be made by choice of the ratio λ/c to match the estimated dispersion. Finally, we note that the particle paths have been observed "long enough" in Section 4.2 from dispersion point of view. The large time behavior for obtaining K appears much earlier in Figures 11 to 16 compared with total observation times in Figures 1 to 9 when the two sets are matched according to their τ_T.

References

1. Çinlar, E. On a Random Velocity Field. Princeton University, Princeton, NJ, 1993.

2. Çinlar, E. Isotropic Velocity Fields of Poisson Shot Noise Type. Princeton University, Princeton, NJ, 1994.

3. Çağlar, M. Simulation of Çinlar Type Flows. Bulletin of the International Statistical Institute, 51st Session Proceedings Book 2, 171-174, August 18-26, Istanbul, 1997.

4. Davis, R.E. Lagrangian Ocean Studies. *Annu. Rev. Fluid Mech.*, 1991, **23**, 43-64.

5. Haynes, R., Barton, E.D. Lagrangian Observations in the Iberian Coas. Tran. Zone. *J. Geophys. Res.*, 1991, **96**, 14731-14741.

6. Kallenberg, O. *Random Measures.* Academic Press, New York, 1983.

7. Piterbarg, L. Short-Correlation Approximation in Models of Turbulent Diffusion. *Stochastic*

Models in Geosystems. Springer-Verlag, New York, 1997.

8. Yaglom, A.M. *Correlation Theory of Stationary and Related Random Functions.* Vol. 1. Springer-Verlag, New York, 1987.

9. Chorin, A.J. *Vorticity and Turbulence.* Springer-Verlag, New York, 1994.

10. Hamming, R.W. *Numerical Methods for Scientists and Engineers.* Second Ed. Dover Pub., New York, 1986.

11. Çağlar, M. Flows Generated by Velocity Fields of Poisson Shot-Noise Type: Lyapunov Exponents. Dissertation, Princeton University, Princeton, NJ, 1997.

12. Carmona, R.A., S.A. Grishin, S.A., Molchanov, S.A. Massively Parallel Simulations of the Transport Properties of Gaussian Velocity Fields. In *Mathematical Models for Oceanography.* Eds. R. Adler, P.Muller, B. Rozovskii. Birkhauser, 1995.

13. Csanady, G.T. *Turbulent Diffusion in the Environment.* D. Reidel Pub. Co., Netherlands, 1973.

14. Zirbel, C.L. Stochastic Flows: Dispersion of a Mass Distribution and Lagrangian Observations of a Random Field. Dissertation, Princeton University, Princeton, NJ, 1993.

15. Press, W.H. et.al. *Numerical Recipes in C*, 2nd Edition. Cambridge University Press, New York, 1992.

K	0.02	0.02	0.04	0.05	0.07	0.07	0.07	0.07
λ/c	0.1	0.1	1	1	10	10	100	100
λ	0.01	0.1	0.01	10^{-3}	0.1	0.01	0.1	0.01
c	0.1	1	0.01	10^{-3}	0.01	10^{-3}	10^{-3}	10^{-4}

Table 1: Summary of the results for typical time $\tau_T = 1$.

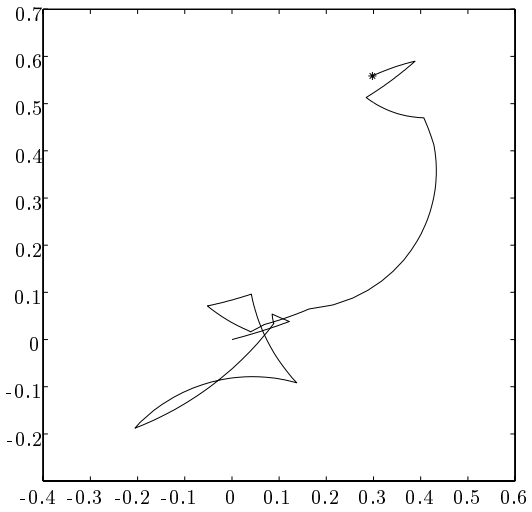

Figure 1: $\tau_E \,/\, \tau_T = 0.1$ $1 \sim \tau_E \ll \tau_T$.

$x_0 = (0,0),\ x_{700} = (0.3, 0.6),\ \ c = 1,\ \lambda = 0.01,\ a \sim$ Unif(-0.54,0.54)

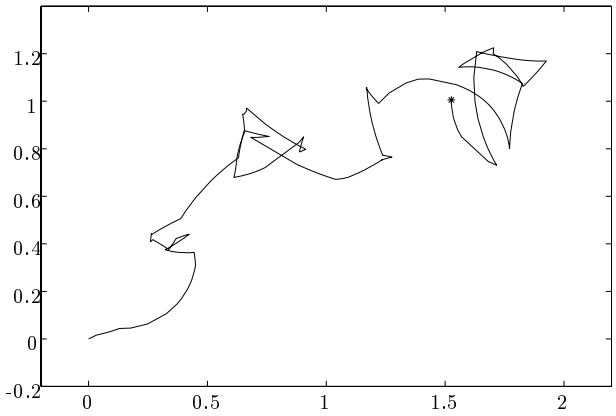

Figure 2: $\tau_E \,/\, \tau_T = 0.1$ $\tau_E \ll \tau_T \sim 1$.

$x_0 = (0,0)$, $x_{250} = (1.5, 1.0),\ \ c = 10,\ \lambda = 0.1,\ a \sim$ Unif(-5.4,5.4)

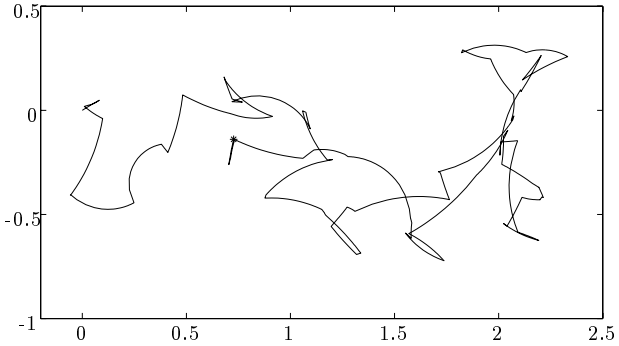

Figure 3: $\tau_E \,/\, \tau_T = 0.1$ $\tau_E \ll \tau_T \ll 1$.

$x_0 = (0,0),\ x_{35} = (0.7, -0.1),\ \ c = 100\ ,\ \ \lambda = 1\ ,\ \ a \sim$ Unif(-54,54)

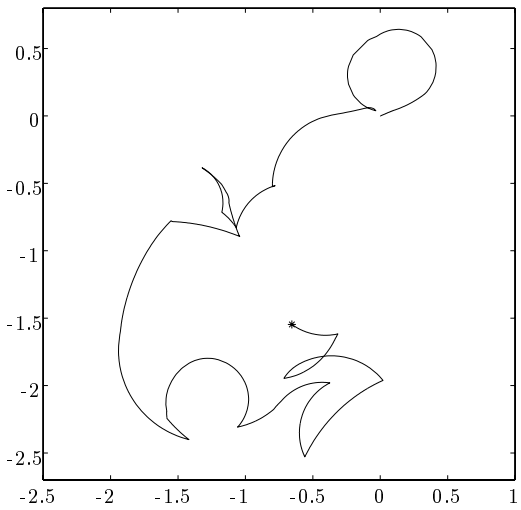

Figure 4: $\tau_E \,/\, \tau_T = 1$ $\tau_E \sim \tau_T \sim 1$.

$x_0 = (0,0),\ x_{80} = (-0.7, -1.5),\ \ c = 1,\ \lambda = 0.1,\ a \sim$ Unif(-1.7,1.7)

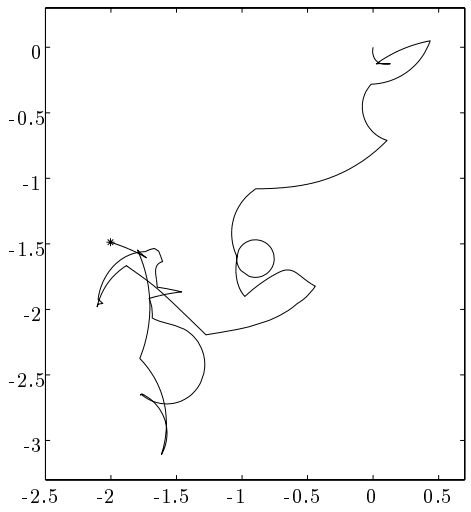

Figure 5: $\tau_E \,/\, \tau_T = 1$ $\tau_T \sim \tau_E \ll 1$.

$x_0 = (0,0)$, $x_{12} = (-2.0, -1.5)$, $c = 10$, $\lambda = 1$, $a \sim$ Unif(-17,17)

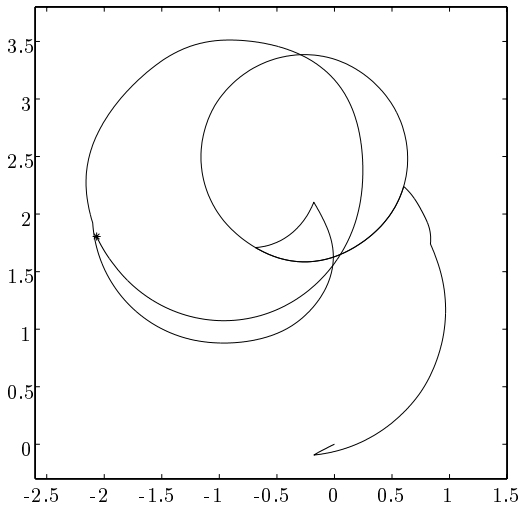

Figure 6: $\tau_E \,/\, \tau_T = 10$ $1 \sim \tau_T \ll \tau_E$.

$x_0 = (0,0)$, $x_{200} = (-2.1, 1.8)$, $c = 0.1$, $\lambda = 0.01$, $a \sim$ Unif(-1.7,1.7)

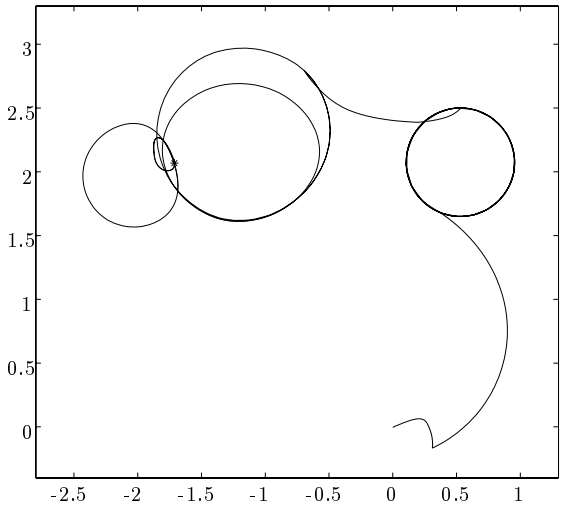

Figure 7: $\tau_E \,/\, \tau_T = 10$ $\tau_T \ll \tau_E \sim 1$.

$x_0 = (0,0)$, $x_{25} = (-1.7, 2.1)$, $c = 1$, $\lambda = 0.1$, $a \sim$ Unif(-17,17)

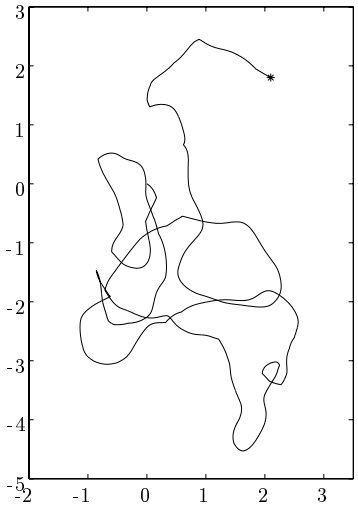

Figure 8: $\tau_E \,/\, \tau_T = 10$ $\tau_T \ll \tau_E \ll 1$.

$x_0 = (0,0)$, $x_2 = (2.1, 1.8)$, $c = 10$, $\lambda = 10$, $a \sim$ Unif(-54,54)

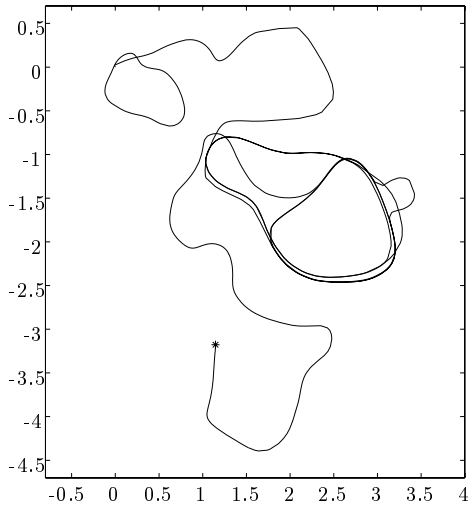

Figure 9: $\tau_E \,/\, \tau_T = 100$ $\tau_T \ll 1 \ll \tau_E$.

$x_0 = (0,0)$, $x_{30} = (1.1, -3.2)$, $c = 0.1$, $\lambda = 0.1$, $a \sim$ Unif(-5.4,5.4)

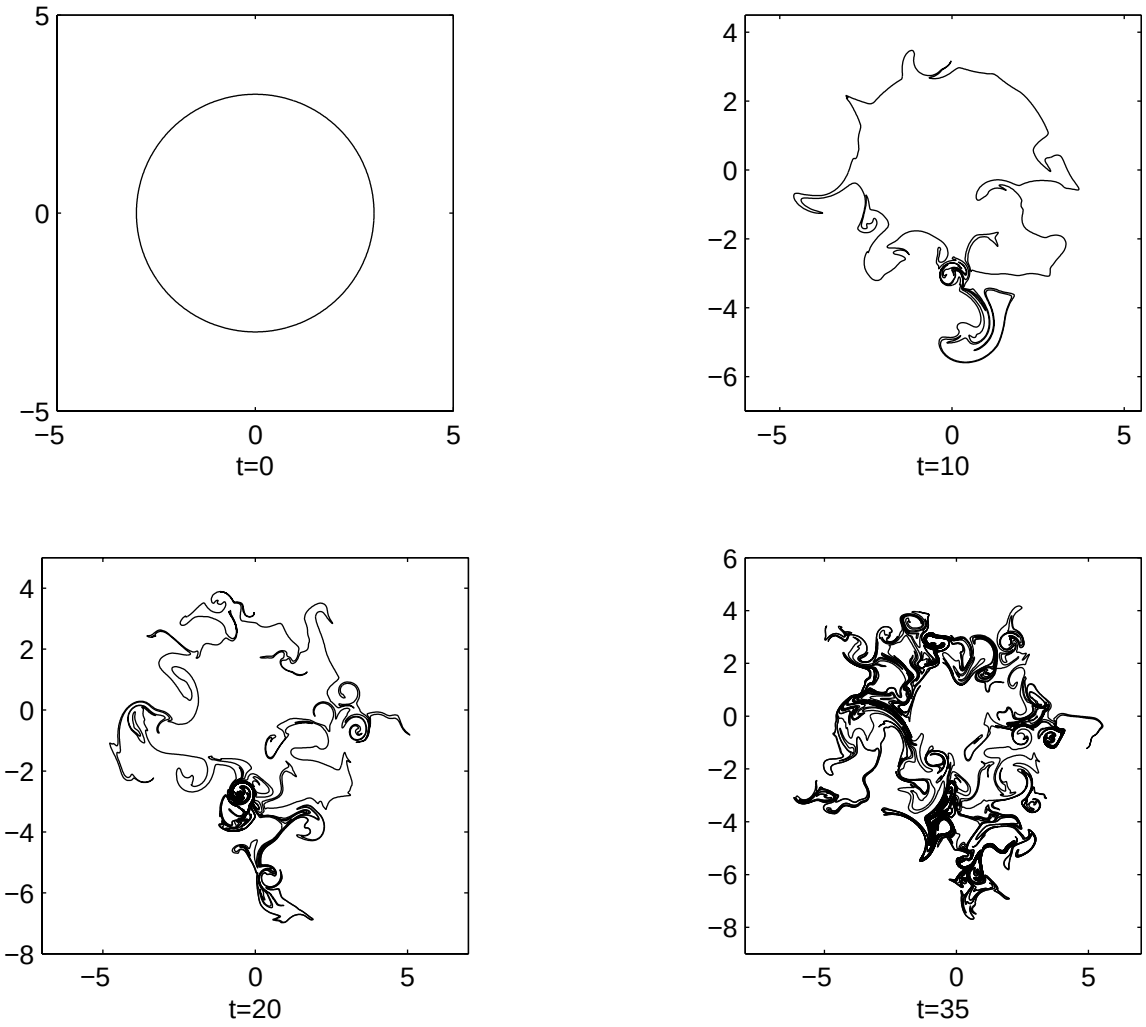

Figure 10: Boundary of an admixture cloud in the flow.

Parameters: $c = 1,\ \lambda = 0.1,\ \ a \sim$ Unif(-1.7,1.7)

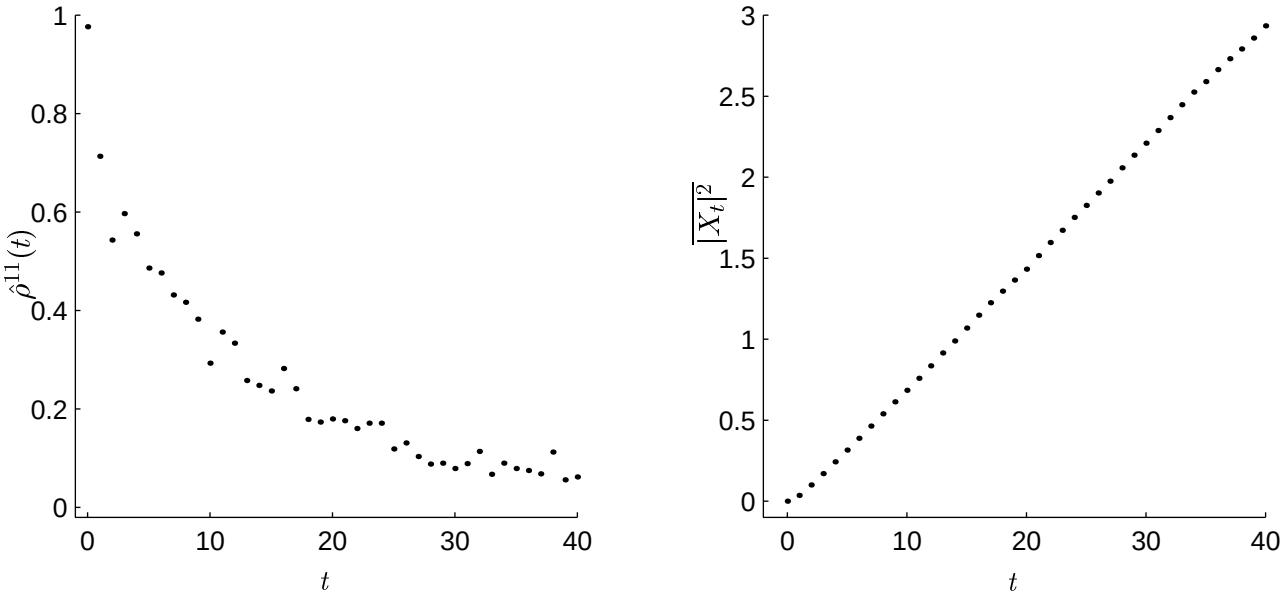

Figure 11: Autocorrelation and dispersion with $c = 1$, $\lambda = 0.1$, $a \sim$Unif(-1.7,1.7) and $\tau_T = 1$.

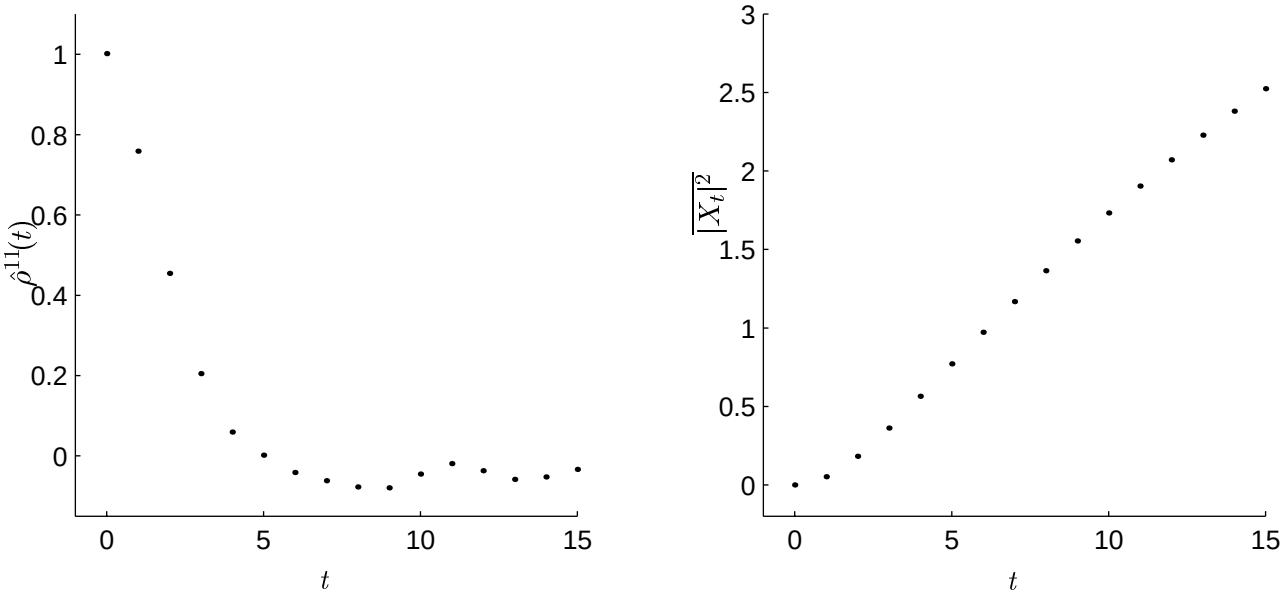

Figure 12: Autocorrelation and dispersion with $c = 0.01$, $\lambda = 0.01$, $a \sim$ Unif(-0.54,0.54) and $\tau_T = 1$.

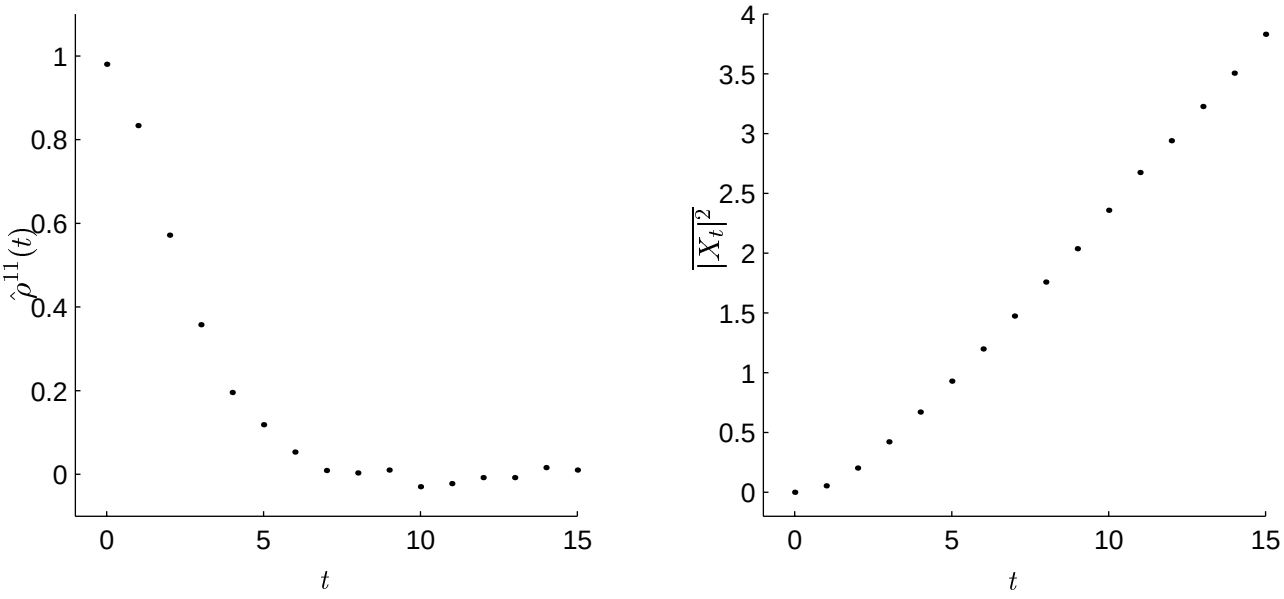

Figure 13: Autocorrelation and dispersion with $c = 0.01$, $\lambda = 0.1$, $a \sim$ Unif(-0.17,0.17) and $\tau_T = 1$.

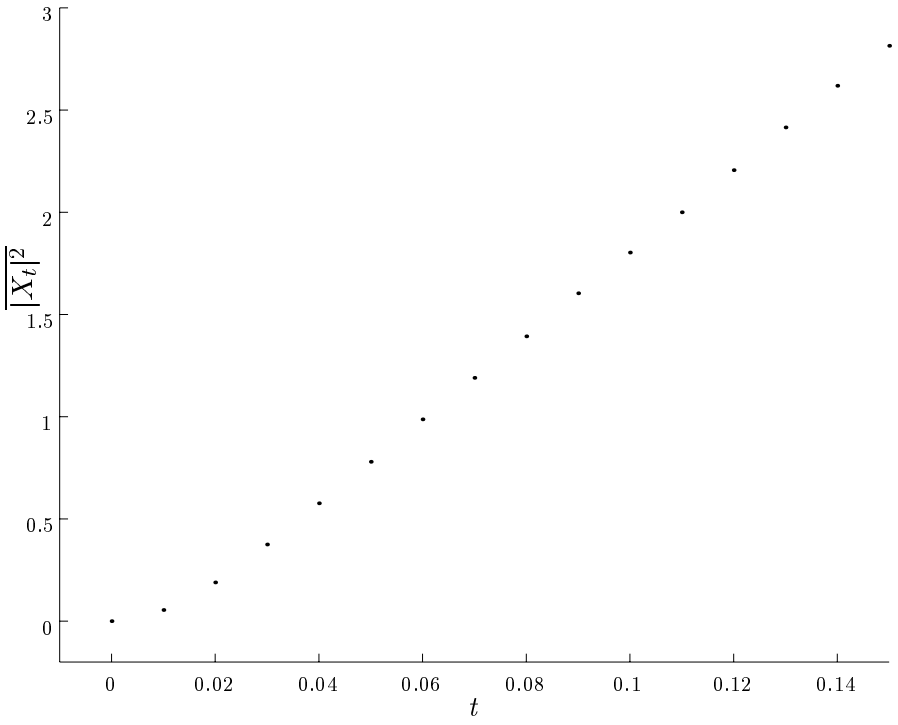

Figure 14: Dispersion with $c = 10$, $\lambda = 10$, $a \sim$ Unif(-54,54) and $\tau_T = 0.01$.

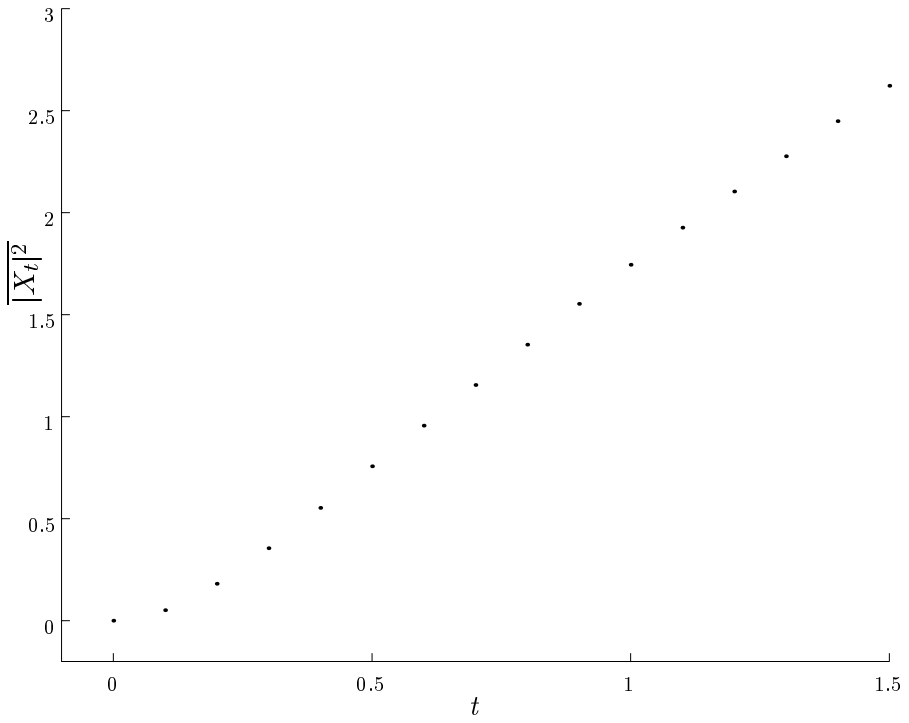

Figure 15: Dispersion with $c = 0.1$, $\lambda = 0.1$, $a \sim$ Unif(-5.4,5.4) and $\tau_T = 0.1$.

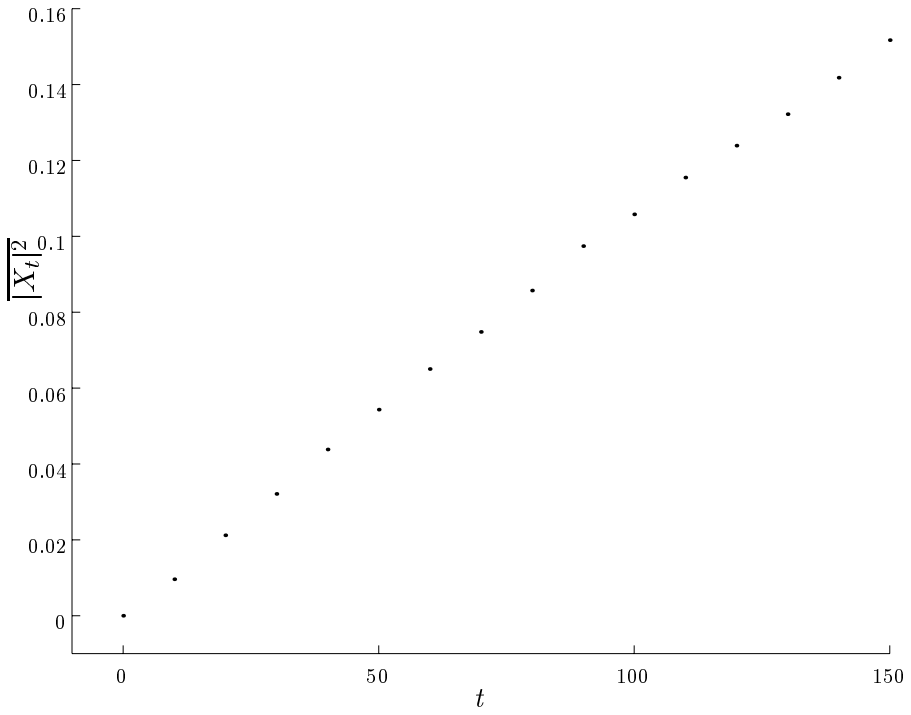

Figure 16: Dispersion with $c = 1$, $\lambda = 0.1$, $a \sim$ Unif(-0.17,0.17) and $\tau_T = 10$.

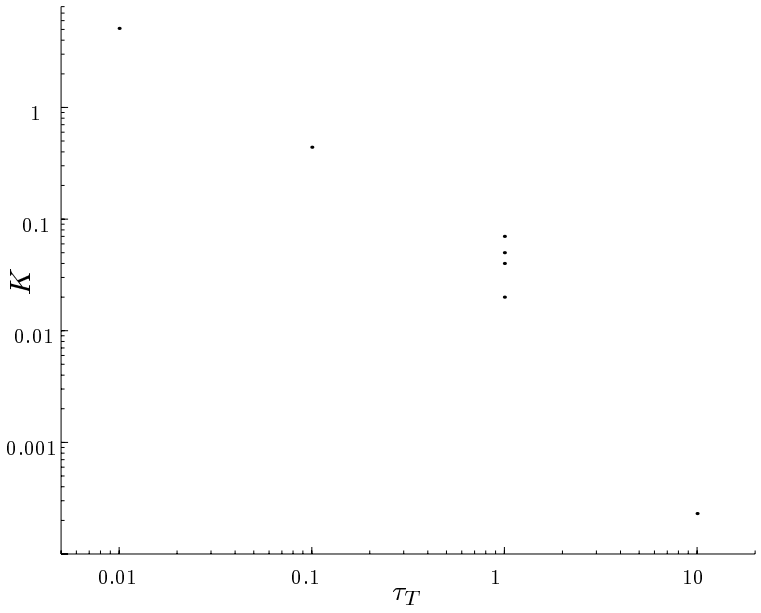

Figure 17: Log-log plot of diffusivity K versus typical time τ_T.